Reports

Formation of Fullerides and Fullerene-Based Heterostructures

D. M. Poirier, T. R. Ohno, G. H. Kroll, Y. Chen, P. J. Benning, J. H. Weaver,* L. P. F. Chibante, R. E. Smalley

Two potassium fulleride phases, metallic K_3C_{60} and nonmetallic K_6C_{60}, are formed when potassium is incorporated into thin C_{60} films under ultrahigh vacuum conditions. Phase separation is observed for intermediate stoichiometries. Results obtained for the C_{60}–K_3C_{60} heterostructure demonstrate that it is stable against potassium migration from the K_3C_{60} phase. In contrast, the C_{60}–K_6C_{60} interface is not stable and K_3C_{60} is formed.

Since it was reported that conducting (*1*) and superconducting (*2–4*) C_{60} solids can be prepared by alkali atom incorporation, several techniques have been used to characterize the phases and properties of the resulting fullerides (*1–11*). The electrical conductivity has now been explained by charge transfer from the alkali atoms to partially fill band states derived from the C_{60} molecular orbitals (*1, 5, 6*). The superconducting phase of K_xC_{60} has been identified ($x \cong 3$) with K ions occupying tetrahedral and octahedral interstitial sites of the face-centered-cubic (fcc) lattice (*3, 8*). K_6C_{60} and Cs_6C_{60} phases have been determined to be body-centered-cubic (bcc) in structure with alkali ions filling the tetrahedral sites (7). It was not clear, however, whether K_xC_{60} was a solid solution or whether samples with stoichiometries $x \neq 3$ were composed of two or more phases. It is particularly important to determine these aspects in order to discuss band filling and superconductivity during K incorporation.

This report focuses on the growth of thin films of K_xC_{60} and Cs_xC_{60} under ultrahigh vacuum conditions so as to determine the phases that form and the stabilities of those phases. With photoemission, we find distinct core level signatures for K_0C_{60}, K_3C_{60}, and K_6C_{60} and conclude that samples with $x \neq 0$, 3, or 6 represent two-phase regions of an equilibrium phase diagram. These phases are readily formed at 300 K in thin films, and we estimate the activation energy for K diffusion. We show that a stable, abrupt heterojunction between C_{60} and K_3C_{60} can be formed. In contrast, the K_6C_{60} phase is less stable, and growth of a C_{60}–K_6C_{60} heterostructure results in K migration and K_3C_{60} formation. Analogous conclusions were reached for Cs_xC_{60}. The relative stability of these phases suggests possibilities for fullerene-based quantum well structures and Josephson junctions.

Fullerenes formed by the contact-arc method were separated by solution with toluene (*12*). Phase-pure C_{60} was obtained by a liquid chromatography process. For thin film growth, it was sublimed from a Ta boat at ~550°C at 1.5×10^{-10} torr onto GaAs(110) surfaces prepared by cleaving. One layer of C_{60} is equivalent to 1.15×10^{14} molecules per square centimeter or ~8 Å nominal deposition. K and Cs were evaporated from outgassed SAES getter sources located ~8 cm from the samples.

The x-ray photoemission (XPS) spectra were obtained with a monochromatized Al K_α x-ray source ($h\nu = 1486.6$ eV, resolution 0.6 eV), while the synchrotron radiation photoemission spectra were obtained with photons from the Aladdin light source (resolution ~0.35 eV). The samples were attached to closed-cycle He refrigerators so that sample temperatures could be varied between 25 K and 470 K. In the XPS measurements, an estimate of the bulk fulleride composition could be made by analysis of the attenuation of substrate features. These estimates were in agreement with compositions determined from K and C core level intensities with corrections for photoionization cross sections. Because the latter method is surface-sensitive, we conclude that the surface composition is representative of the entire film. The surface electronic structure is also representative of the film with charge transfer from K to C_{60} and occupation of levels derived from C_{60} molecular orbitals. For the valence band studies, the stoichiometry was estimated from the emission intensities of band features derived from the highest occupied molecular orbitals (HOMOs) and the lowest unoccupied molecular orbitals (LUMOs) (*5*). No tests for superconductivity were performed, nor were direct determinations of crystal structure made.

Figure 1 shows C 1*s* core level spectra for K deposition onto C_{60} films ~4 layers thick (*10*). The C 1*s* emission from C_{60} is characterized by a sharp peak at 285.0 eV (full width at half maximum, FWHM, 0.65 eV) with shake-up and molecular plasmon features below the main line. The first shake-up at 1.9 reflects a π-π^* transition involving HOMO and LUMO bands induced by the sudden creation of the core hole (*14*). The middle spectrum for K_3C_{60} was obtained for a film grown at 400 K. Equivalent spectra were obtained from films grown at 300 K or annealed to 450 K. We conclude that the K_3C_{60} equilibrium phase was readily achieved at room temperature. The C 1*s* peak appears at 284.6 eV with an asymmetry that is typical of a metal in which electron excitation gives rise to energy losses for the photoelectron. For K_3C_{60}, the K 2*p* emission reveals a pair of spin-orbit-split doublets separated by 1.1 eV, indicating the

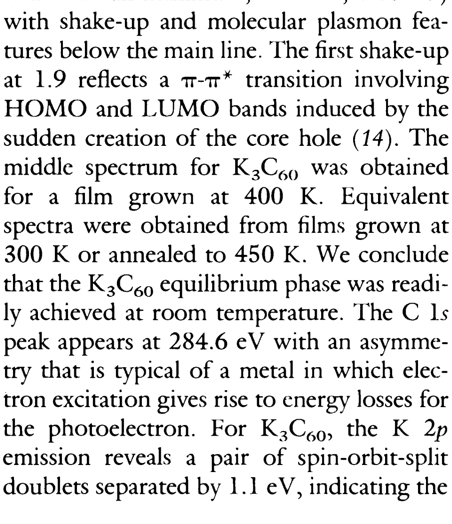

Fig. 1. C 1*s* and K 2*p* core level spectra for K_xC_{60} with average stoichiometries, *x*, as indicated. Dashed lines show decompositions for $x = 1.5$ and 4.5 into contributions from the C_{60}, K_3C_{60}, and K_6C_{60} phases. The K 2*p* core level for $x \leq 3$ shows components that result from K ions in tetrahedral and octahedral sites with a 2:1 ratio.

D. M. Poirier, T. R. Ohno, G. H. Kroll, Y. Chen, P. J. Benning, J. H. Weaver, Department of Materials Science and Chemical Engineering, University of Minnesota, Minneapolis, MN 55455.
L. P. F. Chibante and R. E. Smalley, Rice Quantum Institute and Departments of Chemistry and Physics, Rice University, Houston, TX 77251.

*To whom correspondence should be addressed.

existence of two inequivalent sites for K ions. This is consistent with K occupying the tetrahedral and octahedral interstices in the fcc lattice. The experimental 2:1 intensity ratio corresponds to the expected abundance of the two types of sites, and the energy shift is in agreement with estimates of the bulk Madelung and polarization energies (*13*). Scanning tunneling microscopy studies (*10*) have shown that fulleride films in this thickness regime are terminated in close-packed planes where each C_{60} molecule is surrounded by six threefold hollows. These surface sites correspond to the tetrahedral and octahedral interstices of the bulk lattice. Occupation of all of these hollow sites would result in a K-rich surface which is not observed. Maintaining the K_3C_{60} stoichiometry for the surface C_{60} layer would require filling three-fourths of these hollows. Such a picture would be consistent with our results.

The top spectrum of Fig. 1 shows the C 1*s* and K 2*p* emission for a sample exposed to sufficient K to reach saturation, that is K_6C_{60}. The C 1*s* line, appearing at a binding energy of 284.9 eV, is symmetric with a FWHM, 0.77 eV, that is substantially smaller than for K_3C_{60}. Hence, line shape decomposition for mixed-phase samples is straightforward. For both C_{60} and K_6C_{60}, photoemission involves the removal of an electron from a nonconducting molecular solid, and the response of other electrons to the resulting hole will influence the observed binding energy (*14*). For stoichiometries slightly less than K_6C_{60}, the same sharp C 1*s* line is observed, shifted ~0.7 eV to lower binding energy and the Fermi level cutoff falls within the LUMO-derived band. To account for these final state energy changes, we have shifted the K_6C_{60} spectra for clarity in Fig. 1 (*13*). For K_6C_{60}, the distinct shake-up feature at 1.2 eV corresponds to transitions between the now occupied LUMO-derived and still empty (LUMO+1)–derived bands. We note that inverse photoemission results give a 1.2-eV separation between the LUMO and LUMO+1 bands for pure C_{60} (*13, 15*). For K_6C_{60}, the K emission appears as a single $p_{1/2}, p_{3/2}$ doublet, as would be expected for K occupying the tetrahedral sites of the bcc phase.

Figure 1 shows the spectrum acquired for K_xC_{60} for $x = 1.5$ where the C 1*s* main line can be deconvolved into a sharp peak and a broad shoulder with intensity ratios that indicate the average distribution of K over the 150-μm-diameter probed region. Microscopically, they demonstrate phase separation into surface regions of C_{60} and K_3C_{60}. Again, we conclude that K_3C_{60} nucleates at 300 K. Diffusion should be very easy through the C_{60} phase but it should be more difficult in K_3C_{60} where the interstitial sites are blocked. The spectra in Fig. 1 for $x = 4.5$ can be described by the superposition of K_3C_{60} and K_6C_{60} spectra, as indicated. Since nucleation of the bcc phase requires a martensitic-like transformation and K transport to the nuclei, we expect that growth at 300 K will produce a large number of small grains with a high degree of disorder at their boundaries. Such morphological changes can be inferred from decreased coherence lengths observed in x-ray diffraction experiments (*7*) and have been observed with scanning tunneling microscopy for K_xC_{60}, $x > 3$ (*10*).

These thin film results indicate that the growth of equilibrium structures at 300 K occurs on a time scale that is short because of the high effective mobility of K. The ease of K movement can be quantified by determining the minimum temperature at which K mixes with a C_{60} multilayer. To do this, we formed a metallic K film on GaAs at 25 K and then added three layers of C_{60}. The C 1*s* emission was typical of the clean fullerite phase and the K 2*p* emission was almost completely attenuated. This indicates that the K atoms were retained in the K film (cohesive energy 0.93 eV). Warming to ~100 K resulted in the appearance of small amounts of K, as determined from the K 2*p* emission. By ~200 K, the K 2*p* emission saturated, and the relative energies and line shapes of K and C core levels were indicative of the insulating K_6C_{60} phase. For thin films, the diffusion to produce a K_6C_{60} phase starting with three layers of C_{60} on K is characterized by an effective activation energy of ~0.5 eV. Thus, K diffusion in thin films at 300 K should not present a limitation to the growth of the K_3C_{60} or K_6C_{60} phases under the conditions established in our ultrahigh vacuum experiments.

The evidence supports a model in which films grown at 300 K exhibit distinct equilibrium phases. With this phase diagram in mind, we examined the stability of heterostructures derived from these phases. To produce a C_{60}–K_6C_{60} heterostructure, we deposited C_{60} onto an insulating K_6C_{60} film. The results showed that K diffused into the overlayer and formed a metallic K_3C_{60} phase. This supports the three-phase model since C_{60} and K_6C_{60} are not adjacent phases and a K_3C_{60} layer is expected to form when they are in contact. Since the calculated enthalpies of formation (*9*) for bulk K_3C_{60} and K_6C_{60} both indicate a gain of ~1.1 eV per K atom, the mixing is suspected to be an entropy-driven process.

To examine the C_{60}–K_3C_{60} heterostructure, we annealed a K_3C_{60} sample to maximize its crystallinity and deposited ~3 additional layers of C_{60} at 300 K. In this case, the K_3C_{60} emission was attenuated and there were no line shape changes. A more severe test involved annealing the heterostructure to 440 K. Again, the results showed no changes. We conclude that there was no K diffusion into the C_{60} overlayer and that the interface was abrupt. Moreover, the deposition of even a single C_{60} layer on a similarly prepared K_3C_{60} surface failed to induce line shape changes or K migration during deposition or annealing to 440 K, even though the diffusion length was comparable to that of a lattice constant. Thus, K_3C_{60} is resistant to K vacancy formation, and we conclude that the K_3C_{60} phase is restricted to a narrow composition range. The absence of K redistribution supports the conclusion that C_{60} and K_3C_{60} are the stable phases and that solid solutions do not exist for $0 < x < 3$. This is also consistent with calculated enthalpies of formation of −0.4 and −0.8 eV per K atom for K_1C_{60} and K_2C_{60}, compared to −1.1 eV per K atom for K_3C_{60} and K_6C_{60} (*5, 9*). These results demonstrate the strong tendency of C_{60} to be fully coordinated with charge donors.

Analogous experiments for Cs–C_{60} were undertaken to determine whether these conclusions are applicable to other alkali metal fullerides. Synchrotron radiation photo-

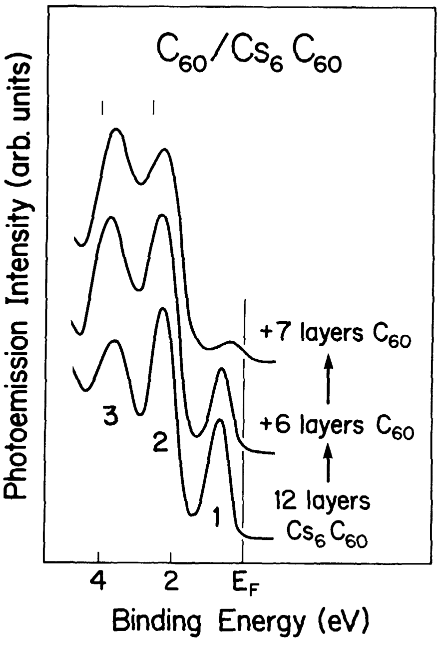

Fig. 2. Valence band spectra for Cs_xC_{60} obtained with $h\nu = 70$ eV. The bottom spectrum shows complete filling of the LUMO-derived band for a 12-monolayer-thick Cs_6C_{60} film. The addition of six layers of C_{60} reduced the nominal stoichiometry to $x = 4$ and intermixing occurred. Following the addition of seven more layers, the intermixed region was covered by a Cs-free C_{60} layer on Cs_3C_{60}. Vertical hash marks indicate the positions of peaks 2 and 3 for the pure C_{60} film.

emission results for Cs deposition on C_{60} at 300 K showed that the C 1*s* core level developed along the general pattern shown in Fig. 1, starting with a sharp main line and π-π^* shake-up features, converting to a broad asymmetric feature where the coverage corresponded to a metallic phase, and terminating with a sharp line and the same satellites seen in Fig. 1 when the Cs_6C_{60} composition was reached. The valence band evolution showed the characteristic growth of a LUMO-derived feature, with broadening and shifting of other filled bands as for K incorporation (*5, 6*). Despite the larger ionic size of Cs compared to K, facile diffusion was observed and phase separation occurred at 300 K for thin films.

Figure 2 shows the valence band emission from a 12-layer-thick Cs_6C_{60} film grown by saturated Cs exposure and annealing to 475 K to remove any excess surface Cs and to improve crystallinity. These results are analogous to those of Benning *et al.* (*5*) and the C 1*s* lineshape is the same as that for K_6C_{60}. The addition of six layers of C_{60} at 300 K resulted in a reduction of the LUMO emission, consistent with Cs redistribution through the 18-layer film with $x = 4$ nominal stoichiometry. The spontaneous outdiffusion of Cs demonstrates that the Cs_6C_{60} layer was unstable in the presence of C_{60}. The broadening in valence band emission, evident by the filling-in of the valley between peaks 2 and 3, can be attributed to overlapping contributions from intimately mixed insulating and metallic phases. The third curve in Fig. 2 shows the valence band emission after addition of seven more layers of C_{60} for a total film thickness of 25 monolayers. In this case, the LUMO-derived band is much weaker than expected for a nominal $Cs_{2.8}C_{60}$ film. This could be explained by formation of a stable Cs_3C_{60} phase, followed by the formation of a C_{60} overlayer free of Cs. This C_{60} layer would attenuate the emission from the metallic phase and contribute intensity at the positions indicated by vertical tic marks in Fig. 2. This scenario would also explain the filling-in of the valley between peaks 2 and 3 and the broadening of peak 3 for the mixed phase. We conclude that a metallic phase forms at the expense of Cs_6C_{60} at the C_{60}–Cs_6C_{60} heterojunction and that this phase is then stable when in contact with C_{60}.

Previous photoemission studies of K_xC_{60} emphasized changes in the valence bands, correctly noting the filling of the LUMO-derived bands (*5, 6*). Here, we have shown that the films produced are two-phase with distinct separation between C_{60} and the K_3C_{60} phases. For growth at 300 K, thermodynamics dictate phase separation, but the details of nucleation and growth produce fine mixtures. Annealing to promote grain growth should produce higher quality samples as desired for superconductivity and electrical characterization. The present results demonstrate that the C_{60}–K_3C_{60} heterojunction is stable and that an analogous structure exists for the Cs_xC_{60} system. C_{60} boundaries with K_6C_{60} or Cs_6C_{60} are not stable. This suggests that insulating-superconducting heterostructures can be fabricated. Such devices are presently under investigation.

REFERENCES AND NOTES

1. R. C. Haddon *et al.*, *Nature* **350**, 320 (1991).
2. A. F. Hebard *et al.*, *ibid.*, p. 600.
3. K. Holczer *et al.*, *Science* **252**, 1154 (1991).
4. M. J. Rosseinsky *et al.*, *Phys. Rev. Lett.* **66**, 2830 (1991).
5. P. J. Benning, J. L. Martins, J. H. Weaver, L. P. F. Chibante, R. E. Smalley, *Science* **252**, 1417 (1991).
6. G. K. Wertheim *et al.*, *ibid.*, p. 1419.
7. O. Zhou *et al.*, *Nature* **351**, 462 (1991).
8. P. W. Stephens *et al.*, *ibid.*, p. 632.
9. J. L. Martins, N. Troullier, M. C. Schabel, in preparation.
10. Y. Z. Li *et al.*, *Science* **253**, 429 (1991).
11. S. Saito and A. Oshiyama, in preparation.
12. R. E. Haufler *et al.*, *J. Phys. Chem.* **94**, 8634 (1990).
13. Unpublished results involving sample preparation and characterization based on photoemission and inverse photoemission for Na, K, and Cs in C_{60} and C_{70} films.
14. J. H. Weaver *et al.*, *Phys. Rev. Lett.* **66**, 1741 (1991).
15. M. B. Jost *et al.*, *Phys. Rev. B*, in press.

16. This work was supported by the Office of Naval Research, the National Science Foundation, and the Robert A. Welch Foundation. The synchrotron radiation experiments were done at Aladdin, a facility operated by the University of Wisconsin for the National Science Foundation.

24 June 1991; accepted 10 July 1991

Interior Structure of Neptune: Comparison with Uranus

W. B. HUBBARD, W. J. NELLIS, A. C. MITCHELL, N. C. HOLMES, S. S. LIMAYE, P. C. MCCANDLESS

Measurements of rotation rates and gravitational harmonics of Neptune made with the Voyager 2 spacecraft allow tighter constraints on models of the planet's interior. Shock measurements of material that may match the composition of Neptune, the so-called planetary "ice," have been carried out to pressures exceeding 200 gigapascals (2 megabars). Comparison of shock data with inferred pressure-density profiles for both Uranus and Neptune shows substantial similarity through most of the mass of both planets. Analysis of the effect of Neptune's strong differential rotation on its gravitational harmonics indicates that differential rotation involves only the outermost few percent of Neptune's mass.

PRIOR TO THE 1989 ENCOUNTER OF the Voyager 2 spacecraft with Neptune, there were only crude constraints on the possible composition and structure of Neptune, and considerable controversy existed about whether Uranus and Neptune's similarity in size and mass extended to their deep interiors. Basic constraints on the interior structure of a rotating liquid planet such as Uranus or Neptune are derived from knowledge of the mass M and equatorial radius at 1-bar pressure a, and the dimensionless zonal gravitational multipole moments J_2, J_4 of the external gravitational potential which arise in response to the planet's rotation (*1–4*), all of which were measured during the 1989 encounter. In this report we focus on inferences about the composition of the deep interiors of Uranus and Neptune which are obtained by comparing admissable pressure-density relations with shock-compression measurements of likely constituent material (*5–7*). We also address the problem of how the interior structure responds to the strong differential rotation which was observed in Voyager 2 images.

Table 1 summarizes our knowledge of the Neptunian interior resulting from the Voyager 2 flyby. The rotation period of the magnetic field (*3*), P_S, is taken to be the solid-body interior rotation period of Neptune. This parameter enters into the calculation of the dimensionless quantity $q = \omega_S{}^2 a^3/GM$, which characterizes the magnitude of the planet's rotational distortion ($\omega_S = 2\pi/P_S$ and G is the gravitational constant). According to the theory of the hydrostatic response of a planet to rotation (*8*), the dimensionless mass quadrupole moment J_2 (normalized to radius a) is to first order

---

W. B. Hubbard, Lunar and Planetary Laboratory, University of Arizona, Tucson, AZ 85721.
W. J. Nellis, A. C. Mitchell, N. C. Holmes, P. C. McCandless, University of California, Lawrence Livermore National Laboratory, Livermore, CA 94550.
S. S. Limaye, Space Science and Engineering Center, University of Wisconsin–Madison, 1225 West Dayton Street, Madison, WI 53706.